

## Application of topological quantum chemistry in electrides

Simin Nie<sup>1,2,\*</sup>, Yuting Qian,<sup>1,3,\*</sup> Jiacheng Gao,<sup>1,3</sup> Zhong Fang,<sup>1,3</sup> Hongming Weng<sup>1,3,4,†</sup> and Zhijun Wang<sup>1,3,‡</sup>

<sup>1</sup>Beijing National Laboratory for Condensed Matter Physics, and Institute of Physics, Chinese Academy of Sciences, Beijing 100190, China

<sup>2</sup>Department of Materials Science and Engineering, Stanford University, Stanford, California 94305, USA

<sup>3</sup>University of Chinese Academy of Sciences, Beijing 100049, China

<sup>4</sup>Songshan Lake Materials Laboratory, Dongguan, Guangdong 523808, China



(Received 31 December 2020; accepted 22 April 2021; published 18 May 2021)

The recently developed theory of topological quantum chemistry (TQC) has built a close connection between band representations in momentum space and orbital characters in real space. It provides an effective way to diagnose topological materials, leading to the discovery of lots of topological materials after the screening of all known nonmagnetic compounds. On the other hand, it can also efficiently reveal spatial orbital characters, including average charge centers and site-symmetry characters. By using TQC theory with the computed irreducible representations in the first-principles calculations, we demonstrate that the electrides with excess electrons serving as anions at vacancies can be well identified by analyzing band representations (BRs), which *cannot* be expressed as a sum of *atomic-orbital-induced* band representations (aBRs). In fact, the floating bands (formed by the excess electrons) belong to the BRs induced from the “pseudo-orbitals” centered at vacancies. In other words, the electrides are proved to be *unconventional* ionic crystals, where a set of occupied bands is not a sum of aBRs, but necessarily contains a BR from vacancies. The TQC theory provides a promising avenue to pursue more electride candidates in ionic crystals.

DOI: [10.1103/PhysRevB.103.205133](https://doi.org/10.1103/PhysRevB.103.205133)

### I. INTRODUCTION

Recently, the discovery of topological materials [1–10] has sprung up, and numerous nonmagnetic materials are predicted to be topologically nontrivial by first-principles calculations based on symmetry-based strategies, such as symmetry indicators [5,6] and topological quantum chemistry (TQC) [7]. To be specific, the TQC theory first builds up the character tables for all  $k$  points, and compatibility relations for all 230 space groups released on the Bilbao Crystallographic Server [11], which make it possible to obtain the corresponding irreducible representations (irreps) of electronic states in the first-principles calculations (i.e., Irvsp [12]). For a given space group, a certain orbital ( $\rho$ , labeled by the site-symmetry group) at sites ( $q$ ) can form a set of energy bands in momentum space (labeled by the irreps of the  $k$ -points’ little groups). This set of irreps at high-symmetry  $k$  points is regraded as a band representation (BR) of  $\rho@q$  in the TQC theory. If a BR  $\rho@q$  is a sum of other BRs, it is not elementary; otherwise, it is an elementary BR (eBR). Then, it constructs a complete list of (e)BRs, serving as its basic building blocks. By matching the irreps for a set of energy bands in a material with those of BRs, one can tell that these bands belong to a certain (e)BR  $\rho@q$ . Thus, it makes a close link between the irreps in momentum space and the orbital characters in real space. The trivial [topological (crystalline)] insulators satisfy compatibility relations and can [cannot] be expressed as a sum of eBRs, while the enforced topological semimetals

violate the compatibility relations. Here, we emphasize that it not only can diagnose the topology of energy bands in momentum space, but also can reveal orbital characters in real space (i.e., the average charge centers and site-symmetry characters) by doing the BR decomposition for a set of energy bands. It is also noted that for topologically trivial insulators, we can further define the *unconventional* ones, whose BR decomposition has to contain an essential BR induced from a “pseudo-orbital” centered at a vacancy, which can be characterized by real-space invariants [13]. In other words, the occupied bands of the *unconventional* insulators (also known as obstructed atomic limits) [7,14] cannot be decomposed as a sum of aBRs (defined as the BR induced by the real atomic orbitals in crystals). To diagnose (topologically trivial) *unconventional* materials by doing the BR decomposition can be widely used in materials science [15–18], such as hydrogen storage materials, higher-order topological insulators (HOTIs), and electrides.

Here we focus on the TQC application in the electrides. Electrides are defined as ionic crystals with excess electrons confined in particular vacancies [19–22], whose arrangement determines the properties of electrides and gives their classification by the dimensionality [23–26]. The anionic electrons, being not attached to any atom, bond, or molecule, exhibit high electron mobility and low work function, which have been experimentally confirmed in  $\text{Ca}_2\text{N}$  [22]: a two-dimensional (2D) electride with an excess electron per unit cell ( $[\text{Ca}_2\text{N}]^+ \cdot e^-$ ). The low work function of electrides is beneficial to induce band inversion and to realize nontrivial band topology [18]. Recently, the concept of electrides with nontrivial band topology has attracted much attention for promising applications in quantum devices [18,27–31]. Given

\*These authors contributed equally to this work.

<sup>†</sup>hmweng@iphy.ac.cn

<sup>‡</sup>wzj@iphy.ac.cn

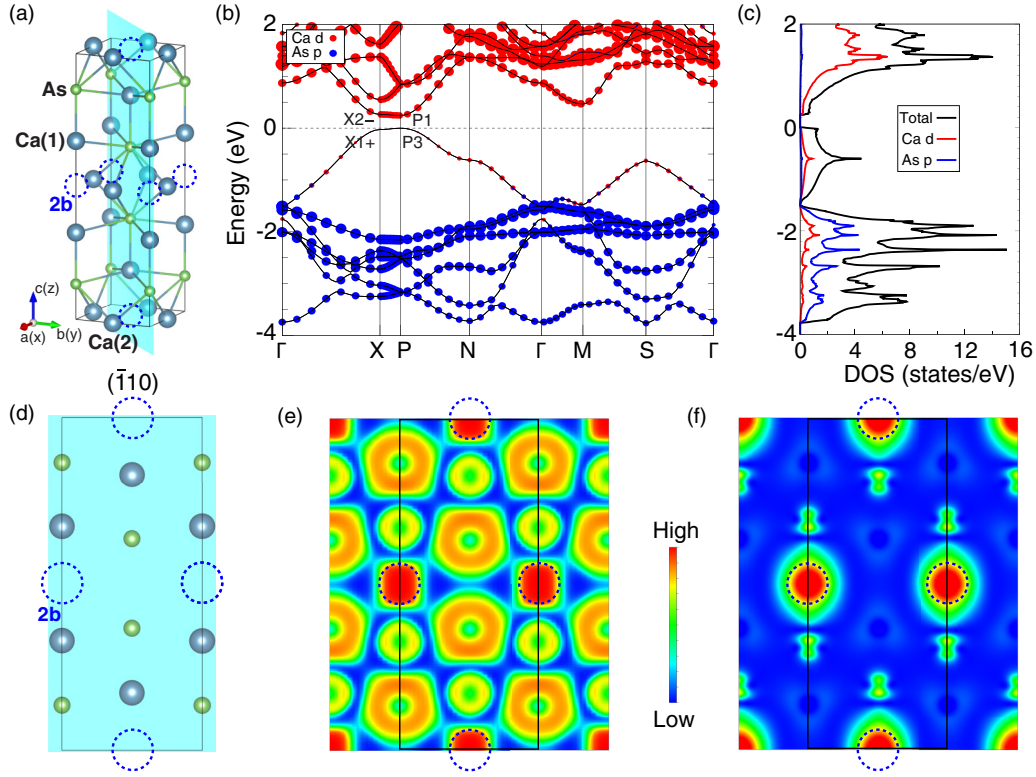


FIG. 1. (a) Crystal structure and (d)  $(\bar{1}10)$  lattice plane of  $\text{Ca}_2\text{As}$ . (b) The mBJ band structure of  $\text{Ca}_2\text{As}$  with spectral weights of Ca- $d$  and As- $p$  orbitals represented by the size of the red and blue circles, respectively. (c) The orbital-resolved DOS of  $\text{Ca}_2\text{As}$ . (e) Electron localization function of the total electron density of  $\text{Ca}_2\text{As}$ , and (f) PED for the states in the energy range  $-1.3$  to  $0$  eV on the  $(\bar{1}10)$  plane of  $\text{Ca}_2\text{As}$ . Hereafter, the corresponding vacancy sites (i.e., WKS  $2b$  for  $\text{Ca}_2\text{As}$ ) are depicted by the blue-dashed circle.

the close relation between BRs and orbital characters, TQC may shed light on the origin of electrides in ionic materials.

Although there are many studies on searching for inorganic electrides, most of them are limited to compute charge distributions [23–26]. The symmetry analysis of electrides is lacking. In this work, the BR analysis of TQC theory provides a way to identify the origin of the bands around the Fermi level ( $E_F$ ) from their symmetry eigenvalues (or irreps) alone, which can be used to find new electride candidates effectively. We first introduce the concept of aBRs, which denote the BRs induced by real atomic orbitals in crystals [32–40]. Then we demonstrate that the electrides are unconventional ionic crystals, whose occupied bands are decomposed as a sum of eBRs, but not a sum of aBRs. This is because the BR decomposition necessarily contains a BR from vacancies (occupied by excess electrons). Lastly, some potential electrides are predicted in ionic crystals by the BR analysis of TQC theory, which can be further checked in future experiments.

## II. CALCULATION METHOD

The Vienna *ab initio* simulation package (VASP) [41,42] with the projector augmented wave method [43,44] based on density functional theory was employed for the first-principles calculations. The generalized gradient approximation of Perdew-Burke-Ernzerhof type [45] was used for the exchange-correlation potential. The cutoff energy for plane wave expansion was set to 500 eV. A  $7 \times 7 \times 7$  Monkhorst-

Pack grid for Brillouin zone sampling was supplied in the self-consistent process. A width of 0.02 eV was adopted in the Gaussian smearing method for Fermi level determination. All the band structures were calculated without considering spin-orbit coupling. In order to get more reliable band structures for the  $\text{Ca}_2\text{As}$  family, more accurate calculations with modified Becke-Johnson (mBJ) potential [46] were performed. The virtual crystal approximation [47] was employed to study the electronic structures of  $\text{K}_2\text{O}_{0.5}\text{F}_{0.5}$  and  $\text{Sr}_6\text{Ga}_{0.5}\text{Ge}_{0.5}\text{N}_5$ . The irreps are computed by the program Irvsp [12,48], and the list of aBRs is given by the program pos2aBR [49] (see details in Supplementary Material [32]).

## III. RESULTS AND DISCUSSION

To achieve an electride, it is empirically known that three criteria should be satisfied: excess electrons, lattice vacancies, and suitable electronegativity of the elements. The previous search [23–26] for electrides was done mainly by analyzing the charge density around  $E_F$ , where electron localization function analysis has proved to be effective. Here, by simply analyzing their symmetry eigenvalues (or irreps) alone at several maximal high-symmetry  $k$  points in first-principles calculations, the BR analysis of TQC theory leads to the clear understanding of three characteristics of electrides. First, the floating bands are induced from the BRs of vacancies, indicating that their average charge densities are located at the vacancies in real space. Second, due to the loose confinement,

TABLE I. Atomic positions and aBRs of the compound  $\text{Ca}_2\text{As}$ .

Atom	WKS( $q$ )	Site symm.	Conf.	Irreps( $\rho$ )	aBRs( $\rho@q$ )
As	$4e$	$4mm$	$4p^3$	$p_z : A_1$ $p_x, p_y : E$	$A_1@4e$ $E@4e$
Ca(1)	$4e$	$4mm$	$4s^2$	$s : A_1$	$A_1@4e$
Ca(2)	$4c$	$mmm$	$4s^2$	$s : A_g$	$A_g@4c$

the floating bands are usually close to the  $E_F$ , which is beneficial to induce the band inversion and nontrivial band topology. Third, the excess anionic electrons in vacancies present a strong hydrogen affinity. The absorption of hydrogen usually moves those floating bands far below  $E_F$  and lowers the total energy.

### A. Band representation of the pseudo-orbitals at voids

We are interested in the compounds in the  $\text{Ca}_2\text{As}$  family. The crystal  $\text{Ca}_2\text{As}$  has a body-centered tetragonal structure and space group  $I4/mmm$  (No. 139). The lattice parameters are  $a = 4.63 \text{ \AA}$ ,  $c = 15.56 \text{ \AA}$ . The As and Ca(1) occupy the Wyckoff sites (WKS)  $4e$  (0, 0,  $z$ ) with  $z = 0.135$  and  $0.328$ , respectively, while Ca(2) is at the  $4c$  (0,  $\frac{1}{2}$ , 0), as shown in Fig. 1 and Table I. It is worth noting that the  $2b$  (0, 0,  $\frac{1}{2}$ ) positions, denoted by blue-dashed circles, are hollow. In the (001) planes, the Ca and As atoms form 2D square lattices of Ca and As, respectively, which are stacked alternatively along the  $z$  direction, as shown in Fig. 1(a).

The band structure of  $\text{Ca}_2\text{As}$  with the mBJ functional is shown in Fig. 1(b), where the size of the red and blue circles represents the weights of Ca- $d$  and As- $p$  orbitals, respectively. In addition to the presence of a global band gap in the band structure, one can also find that the valence bands are dominated by As- $p$  orbitals, while the conduction bands are mainly from Ca- $d$  orbitals. Interestingly, since there are seven valence bands but only six As- $p$  orbitals in a primitive cell, one can notice that the highest valence band in the energy range  $-1.5$  to  $0$  eV is not attributed to either As- $p$  or Ca- $d$  orbitals, which are consistent with the orbital-resolved density of states (DOS), as shown in Fig. 1(c). In what follows, we will show that the band does not belong to any aBR.

To check the orbital characters of the seven well-isolated valence bands in the energy range  $-4$  to  $0$  eV, we have computed the irreps for the high-symmetry  $k$  point and done the analysis of BRs for these valence bands, which are presented in Table II. We find that these bands can be decomposed into a sum of BRs:  $(A_1 + E)@4e \oplus A_{1g}@2b$ . In view of all the aBRs of this compound given in Table I, the BR analysis indicates that the lowest six bands [i.e.,  $(A_1 + E)@4e$ ] are consistent with the states formed by three  $p$  orbitals of As (i.e., WKS  $4e$ ), which agrees well with the fatted band structure [Fig. 1(b)]. Interestingly, the remaining band (i.e.,  $A_{1g}@2b$ ) is contributed from a specific eBR generated by a free electron  $e^-$  located at the vacancy  $2b$ . Therefore, the BR decomposition of  $\text{Ca}_2\text{As}$  is not a sum of aBRs, suggesting that this ionic compound can be an electrified candidate in terms of symmetries and irreps.

The  $A_{1g}@2b$  BR of excess electrons is further checked by the calculated charge density distribution. In Figs. 1(e) and

TABLE II. Irreps and BRs for the seven valence bands of  $\text{Ca}_2\text{As}$ . The BR in bold (i.e., the last row) represents the BR generated by an excess electron  $e^-$  located at vacancies. Hereafter, the irreps are given in the order of increasing energy eigenvalues, and the number in the bracket denotes the degeneracy of the irrep.

	$\Gamma$ ( $GM$ )	$M$	$P$	$X$	$N$
Bands	$GM1 + (1)$	$M1 + (1)$	$P5(2)$	$X4 - (1)$	$N2 - (1)$
	$GM5 + (2)$	$M3 - (1)$	$P5(2)$	$X3 - (1)$	$N1 + (1)$
	$GM1 + (1)$	$M5 + (2)$	$P1(1)$	$X4 + (1)$	$N1 + (1)$
	$GM3 - (1)$	$M5 - (2)$	$P3(1)$	$X1 + (1)$	$N2 + (1)$
	$GM5 - (2)$	$M1 + (1)$	$P3(1)$	$X3 + (1)$	$N2 - (1)$
			$X2 - (1)$	$N1 - (1)$	
			$X1 + (1)$	$N2 - (1)$	
BRs					
$A_1@4e$	$GM3 - (1)$	$M3 - (1)$	$P3(1)$	$X2 - (1)$	$N2 - (1)$
	$GM1 + (1)$	$M1 + (1)$	$P1(1)$	$X1 + (1)$	$N1 + (1)$
$E@4e$	$GM5 - (2)$	$M5 - (2)$	$P5(2)$	$X3 - (1)$	$N1 - (1)$
	$GM5 + (2)$	$M5 + (2)$	$P5(2)$	$X3 + (1)$	$N1 + (1)$
				$X4 - (1)$	$N2 - (1)$
				$X4 + (1)$	$N2 + (1)$
$A_{1g}@2b$	<b><math>GM1 + (1)</math></b>	<b><math>M1 + (1)</math></b>	<b><math>P3(1)</math></b>	<b><math>X1 + (1)</math></b>	<b><math>N2 - (1)</math></b>

1(f), we plot the electron localization function of all valence states and partial electron density (PED) of the states in the energy range  $-1.3$  to  $0$  eV on the  $(\bar{1}10)$  plane for  $\text{Ca}_2\text{As}$ , respectively, which both suggest the existence of excess electron distribution at the WKS  $2b$ . Once the surface termination cuts through the vacancies (i.e., the charge centers of the floating bands), surface states would be expected [18,50]. A similar analysis can also be applied to other well-known electrified  $\text{Ca}_2\text{N}$  [22],  $\text{LaCl}$  [24], and  $\text{Ca}_{24}\text{Al}_{28}\text{O}_{64}$  (called C12A7 for short) [21] (see details in Secs. B and C of the Supplemental Material [32]). Only using irreps at several high-symmetry  $k$  points, the BR analysis of TQC theory tells us that the blue bands belong to the BR from vacancies (i.e.,  $A_{1g}@3b$  for  $\text{Ca}_2\text{N}$ ,  $A_{1g}@3b$  for  $\text{NaCl}$ , and  $A_1@2b$  for C12A7 in Fig. 2), which are formed by excess electrons. It is confirmed by projecting the band structure onto the orbital states of the “empty atom” at the vacancy [22].

### B. Band inversion at the Fermi level

It is well known that topological materials usually have the band inversion near  $E_F$ . Compared with the states constrained by nuclei, the floating states are more conductive, and very close to the  $E_F$ . Given the very likely presence of the band inversion between the floating bands and other energy bands around  $E_F$ , it is natural to expect nontrivial band topology in electrifieds, resulting in the discovery of various topological states in electrifieds. The irrep and BR analysis will show that the band inversion in electrifieds is usually related to the BR of the vacancies.

Here, we take  $\text{Y}_2\text{C}$  with as an example of topological electrifieds. It crystallizes in an anti- $\text{CdCl}_2$ -type structure with the space group of  $R\bar{3}m$  (No. 166). In the generalized gradient approximation calculation [45] [Fig. 3(a)], a band inversion is clearly denoted by the irreps ( $L2-$  and  $L1+$ ) of the two low-

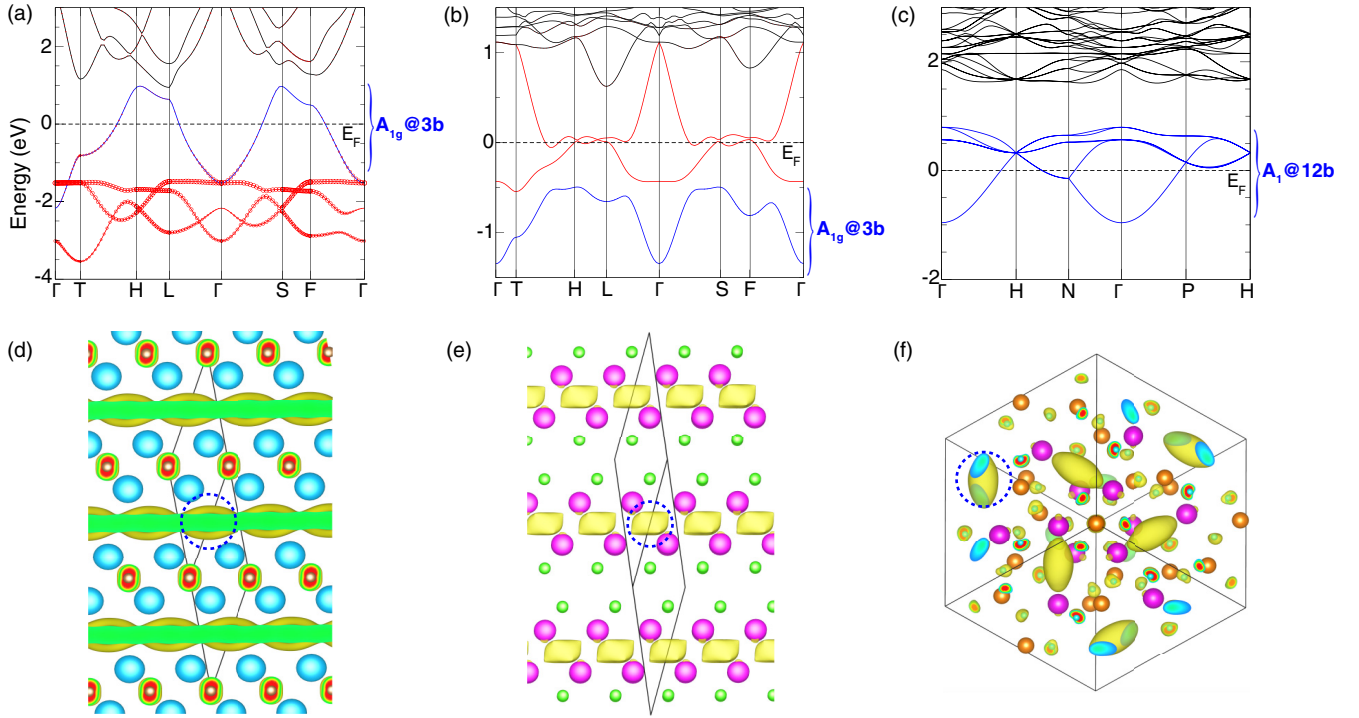


FIG. 2. (a)–(c) The band structures of Ca<sub>2</sub>N, LaCl, and C12A7, respectively. The spectral weight of N *p* orbitals for Ca<sub>2</sub>N is denoted by the size of the red circles. (d)–(f) The calculated PED of the blue-colored bands for Ca<sub>2</sub>N, LaCl, and C12A7 in the energy ranges of [-1.5 eV, 1 eV], [-1.5 eV, -0.5 eV] and [-1 eV, 1 eV], respectively.

energy bands at *L*, which contributes to a nodal-line structure traversing the full Brillouin zone without spin-orbit coupling [18]. The aBRs and the analysis of irreps for Y<sub>2</sub>C are shown in Table III and Table IV, respectively. After replacing the highest valence band irrep *L1+* with “?” (which denotes an arbitrary irrep), the only solution of BR decomposition for the valence bands in Y<sub>2</sub>C is  $(A_{2u} + E_u)@3a \oplus A_{1g}@3b$  with “?” = *L2-*. The aBRs  $(A_{2u} + E_u)@3a$  originate from *C-p* orbitals, while the eBR  $A_{1g}@3b$  is formed by an excess electron at the vacancy site *3b*. The “?” is solved to be *L2-*, suggesting that the Y<sub>2</sub>C has a band inversion at *L*. The PED of the states colored in blue is also explored to confirm its electride feature, as shown in Fig. 3(b). The presence of charge distribution at the vacancies (i.e., WKS *3b*) is consistent with the BR analysis of TQC theory.

The electrides  $A_2B$  ( $A = \text{Ca, Sr, and Ba}$ ;  $B = \text{As, Sb, and Bi}$ ) with the space group of  $I4/mmm$  (No. 139) are also reported topological nodal-line materials without spin-orbit coupling [30,51]. As mentioned above, Ca<sub>2</sub>As is a trivial electride with a global band gap. As the components vary from Ca (As) to Sr (Sb) to Ba (Bi) in the series of materials, the strength of the band inversion changes accordingly. In

TABLE III. Atomic positions and aBRs of the compound Y<sub>2</sub>C.

Atom	WKS( <i>q</i> )	Site symm.	Conf.	Irreps( $\rho$ )	aBRs( $\rho@q$ )
Y	6 <i>c</i>	3 <i>m</i>	5 <i>s</i> <sup>2</sup> 5 <i>d</i> <sup>2</sup>	<i>s/d</i> : $\rho$	$\rho@6c$
C	3 <i>a</i>	-3 <i>m</i>	2 <i>p</i> <sup>2</sup>	<i>p<sub>z</sub></i> : $A_{2u}$ <i>p<sub>x</sub>, p<sub>y</sub></i> : $E_u$	$A_{2u}@3a$ $E_u@3a$

Ba<sub>2</sub>Bi, the band inversion [Fig. 3(c)] gives rise to a nodal line protected by the coexistence of space inversion and time-reversal symmetries. After replacing the highest valence band irreps *X2-* and *P1* of Ba<sub>2</sub>Bi by “?”, we can obtain the highest valence band from the eBR  $A_{1g}@2b$  by solving the BR decomposition. Although the floating band of  $A_{1g}@2b$  is not fully occupied and has a band inversion with the lowest conduction band, Ba<sub>2</sub>Bi can still be considered as an electride with nontrivial band topology. As expected, the PED of Ba<sub>2</sub>Bi shows the charge densities at the vacancy *2b* in Fig. 3(d). In fact, the Ca<sub>2</sub>As family have lots of compounds, which are all electride candidates (see the mBJ band struc-

TABLE IV. Irreps and BRs (copied from TQC) for the four valence bands near the Fermi level of Y<sub>2</sub>C. The question mark (“?”) stands for any 1D irrep (i.e., the arbitrary irrep) at *L*. After analyzing the BRs of the occupied bands, one then find that the arbitrary irrep is solved to be *L2 - (1)*. The BR in bold (i.e., the last row) represents the BR generated by an excess electron *e-* located at vacancies.

	$\Gamma$	<i>T</i>	<i>F</i>	<i>L</i>
Bands	<i>GM2 - (1)</i>	<i>T2 - (1)</i>	<i>F2 - (1)</i>	<i>L2 - (1)</i>
	<i>GM1 + (1)</i>	<i>T3 - (2)</i>	<i>F2 - (1)</i>	<i>L2 - (1)</i>
	<i>GM3 - (2)</i>	<i>T2 - (1)</i>	<i>F1 - (1)</i>	<i>L1 - (1)</i>
			<i>F1 + (1)</i>	? (1)
BRs				
$A_{2u}@3a$	<i>GM2 - (1)</i>	<i>T2 - (1)</i>	<i>F2 - (1)</i>	<i>L2 - (1)</i>
$E_u@3a$	<i>GM3 - (2)</i>	<i>T3 - (2)</i>	<i>F1 - (1) ⊕ F2 - (1)</i>	<i>L1 - (1) ⊕ L2 - (1)</i>
<b><math>A_{1g}@3b</math></b>	<b><i>GM1 + (1)</i></b>	<b><i>T2 - (1)</i></b>	<b><i>F1 + (1)</i></b>	<b><i>L2 - (1)</i></b>

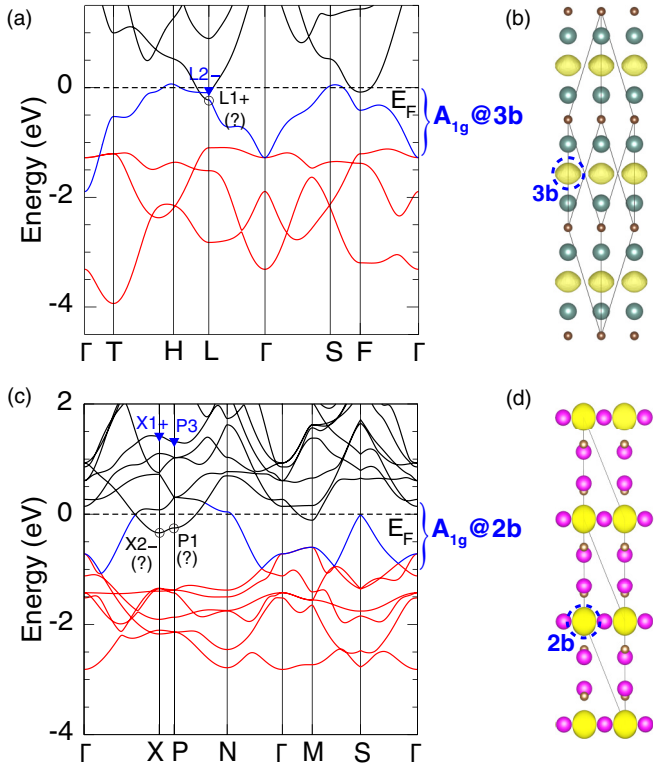


FIG. 3. (a) Band structures of  $Y_2C$  with generalized gradient approximation. (c) Band structures of  $Ba_2Bi$  with mBJ modification. The irreps  $L1+$ ,  $X2-$ ,  $P1$  replaced by “?” can be, respectively, assigned to the irrep  $L2-$ ,  $X1+$ ,  $P3$  marked by blue filled triangles after solving the BR decomposition. The braces show the BRs produced by the bands in the corresponding energy ranges. The PED of the states for (b)  $Y_2C$  and (d)  $Ba_2Bi$  in the energy ranges  $[-1.5 \text{ eV}, 0 \text{ eV}]$  and  $[-1 \text{ eV}, 0.5 \text{ eV}]$ , respectively.

tures for all the compounds in Sec. D of the Supplemental Material [32]).

### C. Hydrogen absorption

The electrides, with excess electrons serving as anions at vacancies, can very easily absorb hydrogen atoms at the vacancies, which would move the floating bands far away from  $E_F$ . In order to understand the absorption process, we show the results of  $Ca_5P_3$  and  $Ba_3CrN_3$  as two paradigms.  $Ca_5P_3$  crystallizes in a  $Mn_5Si_3$ -type structure with the space group of  $P6_3/mcm$  (No. 193), and its electronic structure is shown in Fig. 4(a). The BR analysis shows that these blue-solid bands of  $Ca_5P_3$  are the states formed by excess electrons at vacancies, since the eBR  $A_{1g}@2b$  is determined by the obtained irreps labeled in Fig. 4(a). After absorption of hydrogen atoms at  $2b$  as shown in Fig. 4(c), the floating bands move far below  $E_F$  in  $Ca_5P_3H$  [Fig. 4(b)] because the hydrogen atoms will bond with the surrounding electrons producing a strong interaction, which is consistent with previous work [52]. The similar analysis of  $Ba_3CrN_3$  can be found in Sec. E of the Supplemental Material [32,53]. Therefore, the process of adsorbing hydrogen atoms confirms the results of the BR

analysis, and strongly supports the presence of the excess electrons at vacancies in electrides.

### D. Prediction of electride candidates

Based on the above discussions of three aspects, we find that the BR analysis of TQC theory is very implementable in the understanding of various properties of electrides. We demonstrate that the electrides are unconventional ionic crystals, where a set of energy bands is not a sum of aBRs but necessarily contains a BR from vacancies. Guided by this finding, we apply the BR analysis of TQC to predict some potential electrides in ionic crystals.

We first propose that  $NaBaO$  [54] with the structure of  $P4/nmm$  (No. 129) could be an electride with an excess electron located at the vacancy  $2b$ , as the BR of the floating bands [denoted by blue-colored lines and irreps in Fig. 4(d)] is elementary, and the average charge center is located at the vacancy. In fact, these floating bands are half filled. By absorbing a hydrogen atom at  $2b$  [Fig. 4(f)], the floating bands move completely below  $E_F$  [Fig. 4(e)].

Next, we also find that  $Sr_6GaN_5$  could be an electride after electron doping, i.e.,  $K_2O_{0.5}F_{0.5}$  and  $Sr_6Ga_{0.5}Ge_{0.5}N_5$ . The band structure of  $K_2O$  with space group  $Fm\bar{3}m$  (No. 225) [23] is shown in Fig. 5(a). Above  $E_F$ , we can see that there is an isolated band (blue-colored line) in the energy range 1 to 4 eV. With the obtained irreps at high-symmetry  $k$  points, the BR analysis shows that this band belongs to the eBR of  $A_{1g}@4b$ , which suggests that the band is formed by an excess electron at vacancy  $4b$ . By replacing 50% O with F, the isolated band is partially occupied in  $K_2O_{0.5}F_{0.5}$ . The presence of a spherical charge distribution around the vacancy in the PED of this band [Fig. 5(b)] also suggests that  $K_2O_{0.5}F_{0.5}$  is an electride. Heuristically, we propose that  $Sr_6GaN_5$  with a hexagonal structure of  $P6_3/mcm$  (No. 193) could also be an electride after electron doping. Its band structure is shown in Fig. 5(c). We find two well-isolated conduction bands (blue-colored line) form the eBR of  $A_{1g}@2b$ , indicating the corresponding charge centers at  $2b$ , which are consistent with the calculated PED [Fig. 5(d)]. By electron doping, the floating bands of  $Sr_6GaN_5$  can be reached and become half filled in 50% Ge-doped samples (i.e.,  $Sr_6Ga_{0.5}Ge_{0.5}N_5$ ), as shown in Fig. 5(c). More details of these two predicted materials and the results of another candidate (i.e., electron-doped  $Sr_3P_2$ ) can be found in Sec. F of the Supplemental Material [32].

### E. Discussion

Through the BR analysis of TQC with the obtained irreps at high-symmetry  $k$  points, one can effectively identify the average electronic charge centers and the corresponding site-symmetry characters for a set of separated energy bands, providing an ideal avenue to both understand the essence of the well-known electrides and find new candidates in the future. Our methodology will facilitate the study of the interesting properties of electrides, such as high electron mobility and low work function. More interestingly, more fundamental physical phenomena can be found in the unconventional materials after considering interactions, such as  $Sr_5P_3$  and  $Zr_5Sb_3$ .

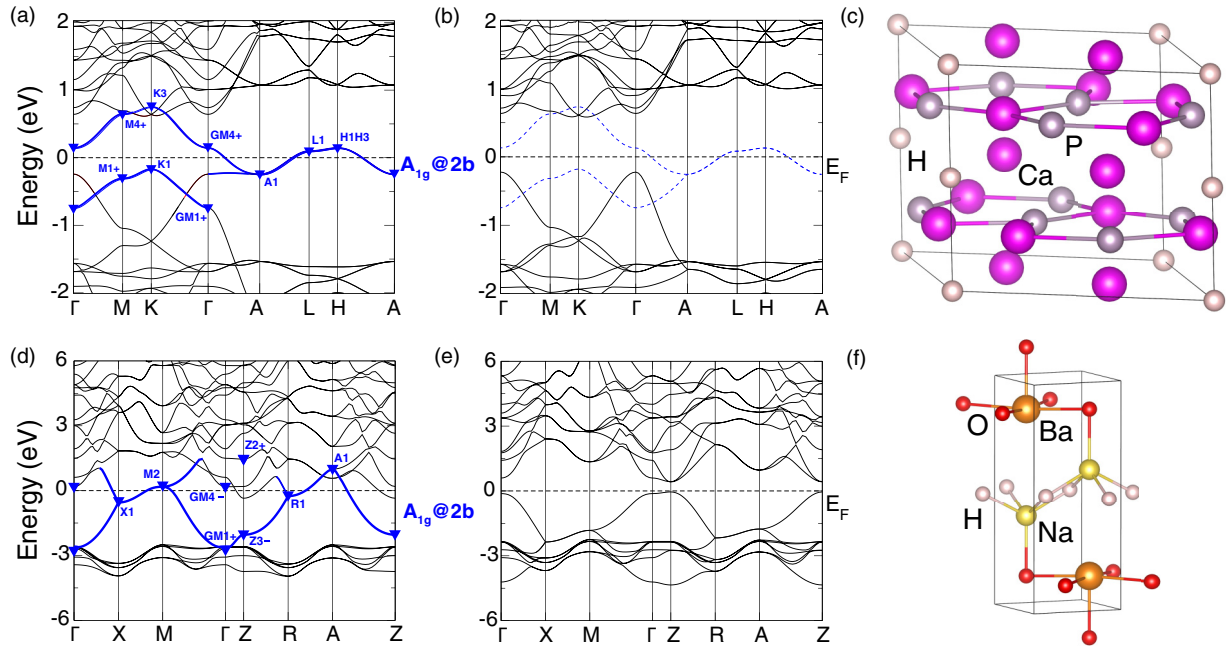


FIG. 4. The band structures of (a)  $\text{Ca}_5\text{P}_3$ , (b)  $\text{Ca}_5\text{P}_3\text{H}$ , (d)  $\text{NaBaO}$ , and (e)  $\text{NaBaOH}$ . The floating bands (blue-solid lines) in  $\text{Ca}_5\text{P}_3$  and  $\text{NaBaO}$  denote electronic states of excess electrons, whose eBRs can be well determined by the obtained irreps. To facilitate the comparison, the irreps of particular bands are marked out, and the floating bands that have “disappeared” for  $\text{Ca}_5\text{P}_3\text{H}$  are depicted by blue-dashed lines in (b). (c),(f) The crystal structures of  $\text{Ca}_5\text{P}_3\text{H}$  and  $\text{NaBaOH}$ , respectively.

The compound  $\text{Sr}_5\text{P}_3$  has two different structures with the space group of  $C2/m$  (No. 12; quasihexagonal form) and

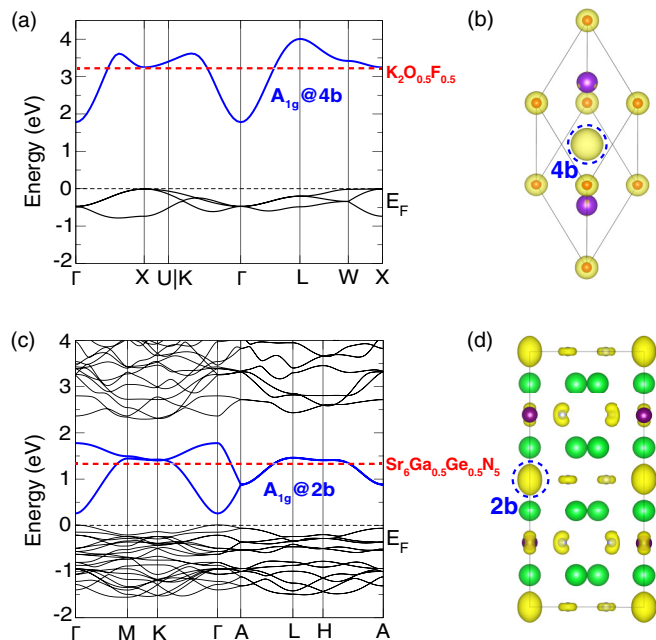


FIG. 5. The calculated band structures and PED of the floating bands (blue-colored lines) for (a),(b)  $\text{K}_2\text{O}$  and (c),(d)  $\text{Sr}_6\text{Ga}_{0.5}\text{Ge}_{0.5}\text{N}_5$ . The PED of the states for  $\text{K}_2\text{O}$  and  $\text{Sr}_6\text{Ga}_{0.5}\text{Ge}_{0.5}\text{N}_5$  in the energy ranges [1 eV, 4 eV] and [0 eV, 2 eV], respectively. The Fermi levels of  $\text{K}_2\text{O}_{0.5}\text{F}_{0.5}$  and  $\text{Sr}_6\text{Ga}_{0.5}\text{Ge}_{0.5}\text{N}_5$  are indicated by red-dashed lines, which are obtained by the virtual crystal approximation as implemented in VASP.

the space group of  $P6_3/mcm$  (No. 193; hexagonal form) at ambient and high pressures, respectively. The atoms in the quasihexagonal form deviate somewhat from that of the hexagonal form, and the hexagonal  $\text{Sr}_5\text{P}_3$  shares the same crystal structure and similar band structure of  $\text{Ca}_5\text{P}_3$ . Thus, they are both expected to be electrides with half-filled floating bands. However, the obtained metallic band structure in the nonmagnetic calculations is in contrast with the observed insulator-type conductivity in experiments [26]. To remedy this discrepancy, the spin-polarized calculation and Coulomb- $U$  effect have been considered in Ref. [26] and a tiny band gap can be found, resulting in the formation of lower and upper Hubbard bands with DOS peaks below and above  $E_F$ , respectively. They conjecture that this material may be a Mott insulator due to the effect of the on-site Coulomb interaction. In addition, the phase transition from the hexagonal form (high pressure) to the quasihexagonal form (ambient pressure) also suggests the presence of a commensurate charge-density-wave transition.

The compound  $\text{Zr}_5\text{Sb}_3$  is experimentally found to be the first superconductor in the large family of compounds with a  $\text{Mn}_5\text{Si}_3$ -type structure (No. 193) [55], which is believed to be due to the electron-phonon coupling. Although the band structure is a little complicated, after carefully checking the irreps of the electronic states [15], we find that their irreps could be decomposed into a sum of BRs:  $(A + B_1 + B_2)@6g$  (Sb atoms),  $(A_1 + E)@4d$  [Zr(1) atoms] and  $A_1'@2a$  (which is hollow). By electron counting, the floating bands of eBR  $A_1'@2a$  are 1/4 filled and create large Fermi surfaces. When the interstitial sites are filled by extra Sb atoms, the experimental measurements have also found that the superconductivity in  $\text{Zr}_5\text{Sb}_{3+x}$  is suppressed. Similar results are

also confirmed in  $Zr_5Sb_3O$  and  $Zr_5Sb_3C$ . These experiments suggest that the superconductivity may be related to the floating electronic states.

#### IV. CONCLUSIONS

In conclusion, we demonstrate that the analysis of irreps and BRs in the TQC theory provides an effective way to identify the origin of the energy bands around  $E_F$  from their symmetry eigenvalues (or irreps) alone, which is extremely useful to find new electride candidates. The electriles are proved to be unconventional ionic crystals, where a set of well-separated energy bands below/around the  $E_F$  is not a sum of aBRs, but necessarily contains a BR from vacancies. In addition, three characteristics of electriles can be well understood in the TQC theory. First, since there are floating bands with charge densities centered at vacancies in real space, surface states could emerge when the surface termination cuts through these vacancies. Second, as the excess electrons show the lack of strong confinement, low work function and floating bands close to  $E_F$  are expected. Consequently, the band inversion and nontrivial band topology are very likely to happen in electriles. Third, the interstitial anionic electrons easily absorb hydrogen atoms, which would move the floating bands far away from  $E_F$  and gain the benefit in total energy.

More generally, the hydrogen storage materials and 2D HOTIs can be known as unconventional metal alloys and covalent compounds with trivial occupied bands being not a sum of aBRs, respectively. Nevertheless, the disagreement between the average charge centers and the atomic positions can be well diagnosed by the BR analysis of TQC theory, which can be widely used in these *unconventional* materials [15], such as electriles, hydrogen storage materials, and HOTIs.

#### ACKNOWLEDGMENTS

This work was supported by the National Natural Science Foundation of China (Grant No. 11974395), the Strategic Priority Research Program of Chinese Academy of Sciences (Grant No. XDB33000000), and the Center for Materials Genome. H.W. acknowledges support from the Ministry of Science and Technology of China under Grants No. 2016YFA0300600 and No. 2018YFA0305700, the Chinese Academy of Sciences under Grant No. XDB28000000, the Science Challenge Project (Grant No. TZ2016004), the K. C. Wong Education Foundation (Grant No. GJTD-2018-01), Beijing Municipal Science & Technology Commission (Grant No. Z181100004218001), and the Beijing Natural Science Foundation (Grant No. Z180008).

- 
- [1] F. Tang, H. C. Po, A. Vishwanath, and X. Wan, *Nature (London)* **566**, 486 (2019).
- [2] F. Tang, H. C. Po, A. Vishwanath, and X. Wan, *Nat. Phys.* **15**, 470 (2019).
- [3] T. Zhang, Y. Jiang, Z. Song, H. Huang, Y. He, Z. Fang, H. Weng, and C. Fang, *Nature (London)* **566**, 475 (2019).
- [4] M. G. Vergniory, L. Elcoro, C. Felser, N. Regnault, B. A. Bernevig, and Z. Wang, *Nature (London)* **566**, 480 (2019).
- [5] H. C. Po, A. Vishwanath, and H. Watanabe, *Nat. Commun.* **8**, 1 (2017).
- [6] Z. Song, T. Zhang, Z. Fang, and C. Fang, *Nat. Commun.* **9**, 1 (2018).
- [7] B. Bradlyn, L. Elcoro, J. Cano, M. Vergniory, Z. Wang, C. Felser, M. I. Aroyo, and B. A. Bernevig, *Nature (London)* **547**, 298 (2017).
- [8] T. H. Hsieh, H. Lin, J. Liu, W. Duan, A. Bansil, and L. Fu, *Nat. Commun.* **3**, 982 (2012).
- [9] Z. Wang, A. Alexandradinata, R. J. Cava, and B. A. Bernevig, *Nature (London)* **532**, 189 (2016).
- [10] J. Ma, C. Yi, B. Lv, Z. Wang, S. Nie, L. Wang, L. Kong, Y. Huang, P. Richard, P. Zhang *et al.*, *Sci. Adv.* **3**, e1602415 (2017).
- [11] Bilbao Crystallographic Server, <https://www.cryst.ehu.es/cgi-bin/cryst/programs/bandrep.pl>.
- [12] J. Gao, Q. Wu, C. Persson, and Z. Wang, *Comput. Phys. Commun.* **261**, 107760 (2021).
- [13] Z.-D. Song, L. Elcoro, and B. A. Bernevig, *Science* **367**, 794 (2020).
- [14] J. Cano, B. Bradlyn, Z. Wang, L. Elcoro, M. G. Vergniory, C. Felser, M. I. Aroyo, and B. A. Bernevig, *Phys. Rev. B* **97**, 035139 (2018).
- [15] Jiacheng Gao, Yuting Qian, and Zhijun Wang (unpublished).
- [16] X.-L. Sheng, C. Chen, H. Liu, Z. Chen, Z.-M. Yu, Y. X. Zhao, and S. A. Yang, *Phys. Rev. Lett.* **123**, 256402 (2019).
- [17] E. Lee, R. Kim, J. Ahn, and B.-J. Yang, *npj Quantum Mater.* **5**, 1 (2020).
- [18] M. Hirayama, S. Matsuishi, H. Hosono, and S. Murakami, *Phys. Rev. X* **8**, 031067 (2018).
- [19] S. B. Dawes, D. L. Ward, R. H. Huang, and J. L. Dye, *J. Am. Chem. Soc.* **108**, 3534 (1986).
- [20] J. L. Dye and M. G. DeBacker, *Annu. Rev. Phys. Chem.* **38**, 271 (1987).
- [21] S. Matsuishi, Y. Toda, M. Miyakawa, K. Hayashi, T. Kamiya, M. Hirano, I. Tanaka, and H. Hosono, *Science* **301**, 626 (2003).
- [22] K. Lee, S. W. Kim, Y. Toda, S. Matsuishi, and H. Hosono, *Nature (London)* **494**, 336 (2013).
- [23] T. Tada, S. Takemoto, S. Matsuishi, and H. Hosono, *Inorg. Chem.* **53**, 10347 (2014).
- [24] Y. Zhang, H. Wang, Y. Wang, L. Zhang, and Y. Ma, *Phys. Rev. X* **7**, 011017 (2017).
- [25] T. TADA, J. Wang, and H. Hosono, *J. Comput. Chem. Jpn.* **16**, 135 (2017).
- [26] J. Wang, K. Hanzawa, H. Hiramatsu, J. Kim, N. Umezawa, K. Iwanaka, T. Tada, and H. Hosono, *J. Am. Chem. Soc.* **139**, 15668 (2017).
- [27] H. Huang, K.-H. Jin, S. Zhang, and F. Liu, *Nano Lett.* **18**, 1972 (2018).
- [28] S. Nie, B. A. Bernevig, and Z. Wang, *Phys. Rev. Res.* **3**, L012028 (2021).
- [29] S.-C. Zhu, L. Wang, J.-Y. Qu, J.-J. Wang, T. Frolov, X.-Q. Chen, and Q. Zhu, *Phys. Rev. Mater.* **3**, 024205 (2019).

- [30] X. Zhang, B. Fu, L. Jin, X. Dai, G. Liu, and Y. Yao, *J. Phys. Chem. C* **123**, 25871 (2019).
- [31] S. Nie, H. Weng, and F. B. Prinz, *Phys. Rev. B* **99**, 035125 (2019).
- [32] See Supplemental Material at <http://link.aps.org/supplemental/10.1103/PhysRevB.103.205133> for the details of the code pos2aBR, irrep and BR analysis of  $\text{Ca}_2\text{N}$  and  $\text{LaCl}$ , irrep and BR analysis of  $\text{C12A7}$ , the evolution of mBJ band structures of  $\text{A}_2\text{B}$ , the absorption of hydrogen atoms in  $\text{Ba}_3\text{CrN}_3$ , and the BR analysis of the predicted electrides, which includes Refs. [33–40].
- [33] A. Togo and I. Tanaka, Spglib: A software library for crystal symmetry search, [arXiv:1808.01590](https://arxiv.org/abs/1808.01590).
- [34] M. G. Vergniory, L. Elcoro, Z. Wang, J. Cano, C. Felser, M. I. Aroyo, B. A. Bernevig, and B. Bradlyn, *Phys. Rev. E* **96**, 023310 (2017).
- [35] J. Cano, B. Bradlyn, Z. Wang, L. Elcoro, M. G. Vergniory, C. Felser, M. I. Aroyo, and B. A. Bernevig, *Phys. Rev. Lett.* **120**, 266401 (2018).
- [36] M. I. Aroyo, J. Perez-Mato, D. Orobengoa, E. Tasci, G. de la Flor, and A. Kirov, *Bulg. Chem. Commun.* **43**, 183 (2011).
- [37] M. I. Aroyo, J. M. Perez-Mato, C. Capillas, E. Kroumova, S. Ivantchev, G. Madariaga, A. Kirov, and H. Wondratschek, *Z. Kristallogr. Cryst. Mater.* **221**, 15 (2006).
- [38] M. I. Aroyo, A. Kirov, C. Capillas, J. Perez-Mato, and H. Wondratschek, *Acta Crystallogr., Sec. A: Found. Crystallogr.* **62**, 115 (2006).
- [39] C. J. Bradley and A. P. Cracknell, *The Mathematical Theory of Symmetry in Solids* (Clarendon, London, 1972).
- [40] J. Wang, X. Sui, S. Gao, W. Duan, F. Liu, and B. Huang, *Phys. Rev. Lett.* **123**, 206402 (2019).
- [41] G. Kresse and J. Furthmüller, *Phys. Rev. B* **54**, 11169 (1996).
- [42] G. Kresse and J. Furthmüller, *Comput. Mater. Sci.* **6**, 15 (1996).
- [43] P. E. Blöchl, *Phys. Rev. B* **50**, 17953 (1994).
- [44] G. Kresse and D. Joubert, *Phys. Rev. B* **59**, 1758 (1999).
- [45] J. P. Perdew, K. Burke, and M. Ernzerhof, *Phys. Rev. Lett.* **77**, 3865 (1996).
- [46] F. Tran and P. Blaha, *Phys. Rev. Lett.* **102**, 226401 (2009).
- [47] L. Nordheim, *Ann. Phys.* **9**, 607 (1931).
- [48] [https://github.com/zjwang11/irvsp/blob/master/src\\_irvsp\\_v2.tar.gz](https://github.com/zjwang11/irvsp/blob/master/src_irvsp_v2.tar.gz).
- [49] [https://github.com/zjwang11/UnconvMat/blob/main/src\\_pos2aBR.tar.gz](https://github.com/zjwang11/UnconvMat/blob/main/src_pos2aBR.tar.gz).
- [50] I. Tateishi, *Phys. Rev. B* **102**, 155111 (2020).
- [51] X. Zhang, Z.-M. Yu, Y. Lu, X.-L. Sheng, H. Y. Yang, and S. A. Yang, *Phys. Rev. B* **97**, 125143 (2018).
- [52] L. S. Xie, L. M. Schoop, E. M. Seibel, Q. D. Gibson, W. Xie, and R. J. Cava, *APL Mater.* **3**, 083602 (2015).
- [53] N. W. Falb, J. N. Neu, T. Besara, J. B. Whalen, D. J. Singh, and T. Siegrist, *Inorg. Chem.* **58**, 3302 (2019).
- [54] J. Deng, J. Guo, and X. Chen, *J. Am. Chem. Soc.* **142**, 5234 (2020).
- [55] B. Lv, X. Y. Zhu, B. Lorenz, F. Y. Wei, Y. Y. Xue, Z. P. Yin, G. Kotliar, and C. W. Chu, *Phys. Rev. B* **88**, 134520 (2013).